Environ Earth Sci (2013) 69:2779–2797
DOI 10.1007/s12665-012-2098-9

ORIGINAL ARTICLE

Evaluating freshwater lens morphology affected by seawater intrusion using chemistry-resistivity integrated technique: a case study of two different land covers in Carey Island, Malaysia

M. F. Tajul Baharuddin · A. R. Othman · S. Taib · R. Hashim · M. H. Zainal Abidin · M. A. Radzuan

Received: 26 June 2011 / Accepted: 29 October 2012 / Published online: 18 November 2012

Abstract Freshwater lenses are vital to small island communities but are susceptible to seawater intrusion due to the physical changes in the shoreline land cover. The effect of seawater intrusion and irrigation water on a coastal unconfined aquifer beneath naturally preserved mangrove and deforested mangrove-barren belt was investigated in Carey Island. Analysis of the total dissolved solids (TDS) and earth resistivity (ER) using a geochemistry-electrical integrated technique gave a TDS–ER relationship capable of predicting freshwater lens morphology affected by sea-irrigation water. The study result shows freshwater was fourfold thicker in close proximity of the mangrove forest than the mangrove barren area; the further the shoreline from the mangrove thickest section, the less vulnerable was the seawater intrusion and the more fresh the irrigation water, and hence the greater the freshwater availability potential.

Keywords Freshwater lens · Mangrove · Seawater intrusion · Earth resistivity · TDS

M. F. Tajul Baharuddin (✉) · R. Hashim
Department of Civil Engineering, Faculty of Engineering, University of Malaya, 50603 Kuala Lumpur, Malaysia
e-mail: mdfaizal@uthm.edu.my

M. F. Tajul Baharuddin · A. R. Othman · M. H. Zainal Abidin · M. A. Radzuan
Department of Water and Environmental Engineering, Faculty of Civil and Environmental Engineering, Tun Hussein Onn University, 86400 Batu Pahat, Johor, Malaysia

S. Taib
Department of Geology, Faculty of Science, University of Malaya, 50603 Kuala Lumpur, Malaysia

Introduction

Carey Island is a populated ex-promontory island, named after a British agriculturist, Edward Valentine Carey. The island is located at the mouth of the Langat River, separated from the mainland by the Klang River in the north and the Langat River in the east. The Island with a total area of 16,187 ha (6 % of the Langat River Basin) (Figs. 1, 2) (JICA and DMGM 2002) is heavily cultivated with oil palm (10,552 ha) mostly in the coastal region; other land use comprises state land/settlements (4,310 ha) and mangrove forest reserve (1,877 ha) (Golden Hope Plantation Berhad 2006).

JICA and DMGM (2002) reported on the location of the area in the Langat River Basin (Fig. 1), which is hit by the northeast and southwest monsoons annually. The northeast monsoon is from November to March, whereas the southwest monsoon is from May to September. Rainfall intensity varies, most of the rain falling in April and November, with a mean rainfall of 280 mm. The least rain falls in June, with a mean rainfall of 115 mm. Wet seasons are in the transitional periods of the monsoons: March to April and October to November. Monthly rainfall average is 180 mm, whereas annual precipitation is approximately 2,400 mm (JICA and DMGM 2002). From analysis of Carey Island's local precipitation events and monthly rainfall data from 2000 to 2010, two seasons can be deduced: wet (August to December, mean 280 mm) and dry (February to March, mean 150 m) (Mohamad Faizal et al. 2011).

The island's groundwater resource relies substantially on its coastal aquifers for the domestic and cultivation requirements, which must remain sustainable without overexploitation under the threat of seawater intrusion. As groundwater demand increases under the tenth Malaysian

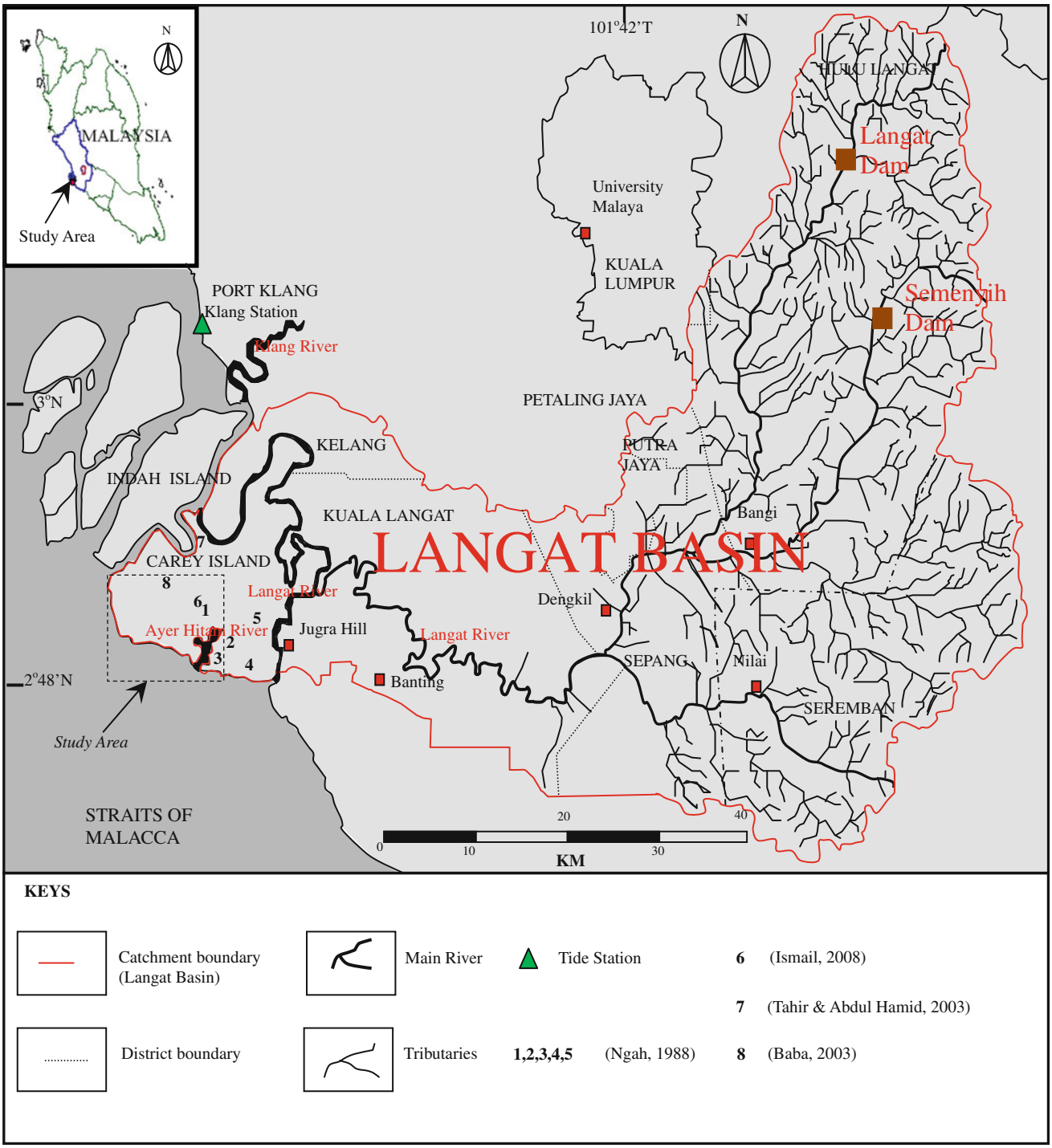

Fig. 1 Location Map of Carey Island in the Langat River Basin. Numbers denote names of villages: *1* and *6* Sg. Judah; *2* Sg. Rambai; *3* Kenanga; *4* Kepau Laut; *5* Sg. Bumbun; *7* West Estate; *8* Sg. Tinggi

Plan (2011–2015) development stress, it is timely to investigate the groundwater status and the influence of intruding seawater and irrigation water on freshwater under natural renewal and supply needed to support the island's eco-systems (GOM 2010). A coastal unconfined aquifer was the subject of investigation involving two distinctively different land covers, a naturally preserved mangrove forest and a severely deforested, eroded mangrove free coastal belt. Both the study sites directly confront the sea of the Straits of Malacca, implying the groundwater problems facing the island authorities might not seem as straightforward as for an ordinary sea-island, because Carey Island

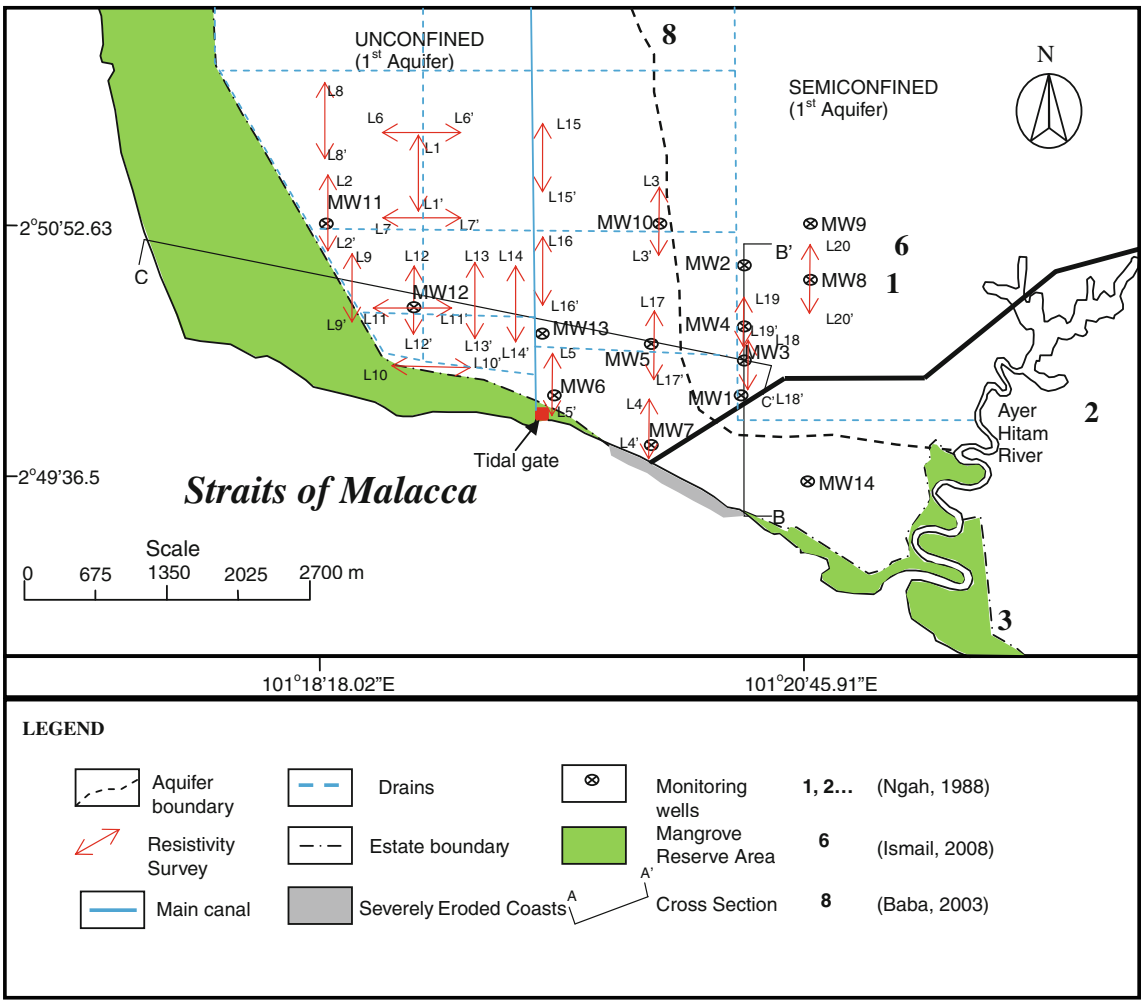

Fig. 2 Locations of monitoring wells and resistivity lines with respect to drainage system in the unconfined and semi-confined aquifers

is ex-promontory (JICA and DMGM 2002). Such problems could have far-reaching effects on the island's the oil palm cultivation (the island's major income) as well as the domestic supply. The most recent concern is about rise in sea level that could affect the island's freshwater morphology due to seawater intrusion (IPCC 2007; Vaeret et al. 2009), which can aggravate due to the changing shoreline caused by the monsoon waves imparting major coastal erosion leading to consequent loss of mangrove cover. Reported loss of natural vegetation from barrier islands in Florida has influenced groundwater recharge to the extent of thinning down the freshwater lenses available in the islands (Schneider and Kruse 2003, 2006).

The best geophysical method for seawater intrusion mapping in particular is the geo-electrical method (Loke 2010a). The geo-electrical method is unique as it detects increased aquifer conductivity via increased pore-water conductivity (Abdul Nassir et al. 2000). Various researchers around the world have applied the geo-electrical method to demarcate coastal-area hydrology conditions, ever since the development of the interpretation technique by Loke and Barker (1996): for example, Schneider and Kruse (2003, 2006)in estimating the freshwater–groundwater interface as a check on their simulation results; Benkabbour et al. (2004) on saltwater intrusion evaluation in the Plioquaternary consolidated coastal aquifer of the Mamora Plains in Morocco; Maillet et al. (2005) in determining the infilling dynamics of the Pegoulier Channel in the Rhone Delta, France; Sathish et al. (2011) on the mixing effect of seawater with groundwater in the Chennai coastal aquifer, India; and in the local Malaysian scenario, Baharuddin et al. (2009) in the study of environmental impact affected by shoreline changes in Selangor, Malaysia.

Several studies have also attempted using the geo-electrical method combined with the geo-chemical method: for example, Di Sipio et al. (2006) for improved salinity interpretation in the Venice estuaries; Awni (2006) for detection of freshwater–saline water interface in the alluvial shoreline of the Dead Sea, Jordan; Sherif et al. (2006) for delineation of seawater intrusion in Wadi Ham, UEA;

Adepelumi et al. (2009) for fresh-saltwater delineation using a vertical-electrical-sounding technique in the Lekki Peninsula in Lagos, Nigeria.

This present work has employed the same technique integrating the geo-electrical method with the geo-chemical method. Highlight on the island's changing physical characteristics forms background to the study (Golden Hope Plantation Berhad (2006), and Affandi et al. (2010)), which provides an insight into the results of the study on groundwater chemistry.

Geological and hydrogeological settings

The study area (Mohamad Faizal et al. 2011) geologically comprises Holocene-age marine sediments (Gula Formation), similarly found in the coastal regions of West Peninsular Malaysia (Suntharalingam and Teoh 1985 and Baba 2003). The sediments consist of grey clay, sand, and minor gravel with fragmented shells and peaty materials. There is one granitic rock outcrop located in the Jugra Hills by the Langat River. Past studies revealed some chemical characteristics of the coastal groundwater aquifers. For instance, Ngah (1988) found freshwater in 15 m deep wells and saline–brackish water in shallower wells (<15 m deep) with chloride exceeding 250 mg/L. Also Tahir and Abdul Hamid (2003) found brackish water in their 96-m-deep well with chloride >250 mg/L. Ismail (2008) found saline–brackish water much deeper (185 m) with conductivity exceeding 2,000 μS/cm. Apart from the groundwater chemical properties, these studies confirm the presence of semi-confined aquifer in two layers (lower and upper) and the absence of confined layer in the study area with freshwater overlying brackish water.

No detailed studies have thus far been carried out on the island's hydrological connection with the mainland. However, the island's groundwater and that of the mainland show dissimilarities which have been described in the following studies. The mainland's coastal regions have been reported to have freshwater 45 m deep in the Simpang Formation (Pleistocene Age) with high chloride contents (2,300–5,800 mg/L) decreasing to below 10 mg/L landward in the hilly regions (Figs. 3, 4) (JICA and DMGM (2002). The saline–brackish water seemed to have inclined interfaces landward as a result of seawater intrusion coming from the Straits of Malacca restricting regional freshwater in the semi-confined aquifer from reaching the aquifer further up the coast. As with the island, Ngah (1988) found freshwater in the 15-m zone in the coastal alluvial deposits of the Gula Formation (Holocene Age) and in the aborigine settlements (Sg. Judah) in the 5- to 7-m formation below the 25-m zone in the semi-confined aquifer where the freshwater and saline water are separated by a horizontal interface (Fig. 5). These observations and the shape of the saline–brackish water interfaces in particular, provide confirmatory evidence of flow discontinuity between the mainland and the study area, which point to but one conclusion: the island and the mainland are hydrologically disconnected.

Island formation impact

The Island located in the Langat Basin (Fig. 1) either got separated from the mainland by the pirates' activities in the nineteenth century or by the Chinese traders who broke the strip of land separating the Langat River on the east and the Straits of Malacca on the west (Golden Hope Plantation Berhad 2006). This land strip now widened by the natural environmental forces, and the irrigation dykes, drainage bunds and tidal gates available collectively form the island's present-day features. Hydrologically, the most significant change has been the cut-off surface runoff that once flowed to the study area from the Langat upper catchment. The Island geologically comprises Quaternary deposits (Suntharalingam and Teoh 1985) with an almost flat coastal topography 1.5–1.8 m above mean sea level (Mohamad Faizal et al. 2011) with hardly any catchments of freshwater from precipitation. The nearest catchment to the study area is the Jugra Hill on the east, which contributes to the salinity and brackishness of the area's agricultural drainage. The island is low lying on the northern side, being 2 m below mean sea level (Golden Hope Plantation Berhad 2006), a feature contributing to the saline–brackish water in the area's drainage system. Most freshwater possibly comes from the mainland's base flow, in addition to possible direct infiltration from precipitation occurring at some point in the unconfined aquifer. Freshwater supply from surface hydrology in the island can become acute as the island is at the edge of the Langat Basin (Fig. 1) with surface water passage being hindered from the upper catchments of the Langat River on the east.

Vegetation pattern impact

Mangrove swamps mostly occupied the island's coastal areas before 1900, which, however, gave way to rubber and oil palm cultivation beginning 1955, following the British colonial interest in the oil palm industry (Golden Hope Plantation Berhad 2006). Coconut plantation in the coastal region was common but where mangrove remains for tidal protection, the coconut trees have literally moved further inland past the mangrove line.

The island's present-day land use is shown in Fig. 6, incorporating the 1974 topographic map of the Department of Survey and Mapping, Malaysia and the 2010 map accessible from the Google. New agriculture land is in the south

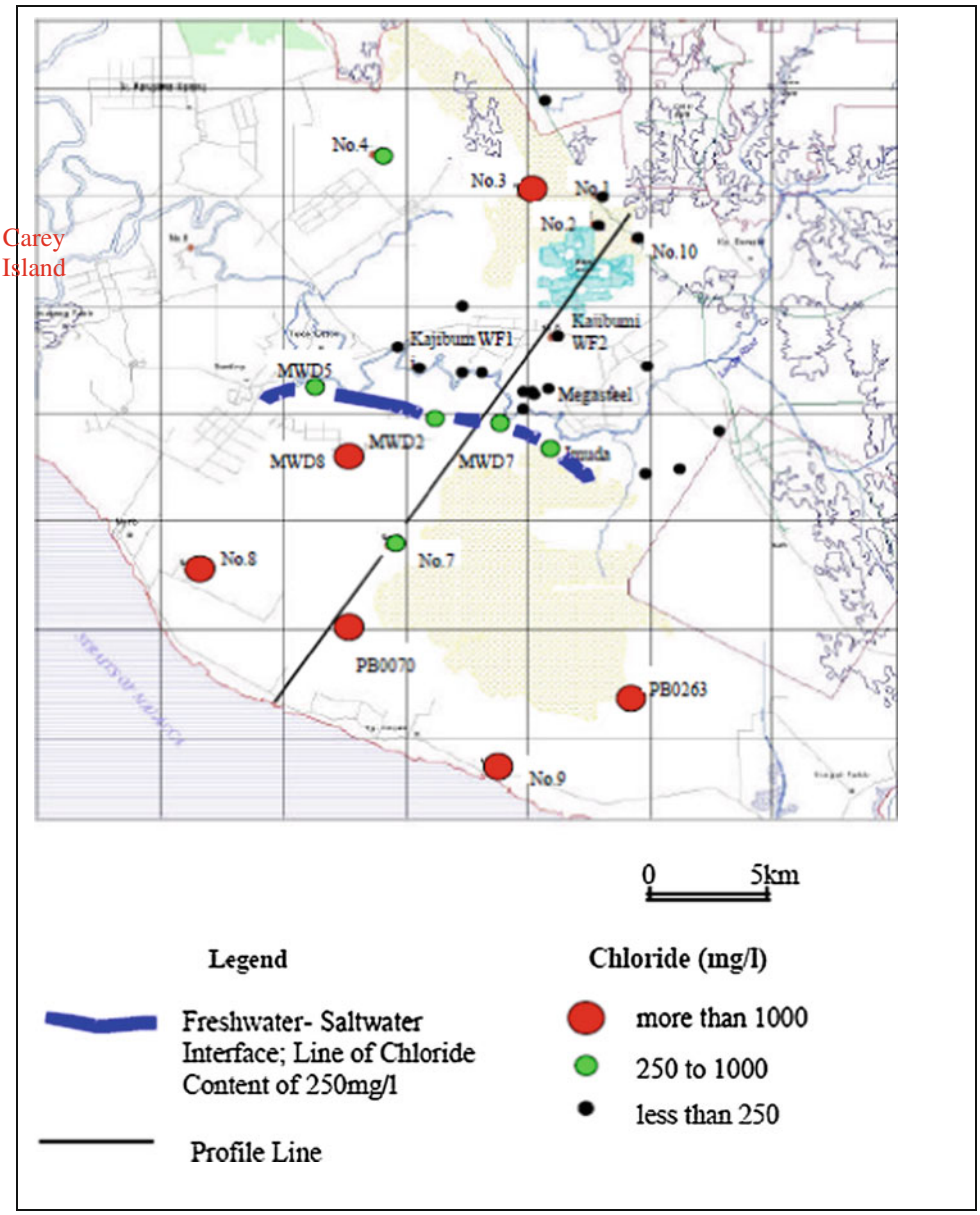

Fig. 3 Saline–freshwater interface in Langat Basin mainland, 15 km from the shoreline

where much mangrove (2,884 ha) has been deforested, evidently shown by the mangrove stumps 300 m into the sea, a result of monsoon (southwest/northeast) waves which encourage coastal soil erosion but suppress mangrove growth (Affandi et al. 2010). Considering the entire island first had 16,187 ha of mangrove before 1900 and 1,876 ha of mangrove forest reserve in the present time, mangrove loss of 88 % can be estimated due to land opening and sea-wave devastation, which is regarded as loss of barrier to seawater intrusion. This problem could worsen in the south but may be controlled in the west, taking advantage of 1,800 ha of mangrove still intact to this day. This requires planning and knowledge with which to contain seawater intrusion that threatens the coastal groundwater aquifers for water supply and oil palm cultivation requirements.

Water supply condition

It was the island aborigines and estate villagers who first used groundwater using primitive hand-pumps. Piped-water supply came in late 1990s, travelling 150 km from the Langat Dam and Semenyih Dam (Fig. 1) through the oil palm cultivation, the Putrajaya, the Multimedia Super Corridor, and finally the Kuala Lumpur International Airport before reaching the Island at journey's end, strained and inadequate (Suratman 2005). In water demand studies (Tahir and Abdul Hamid 2003), water shortage of 1.0 Mm^3/day was projected for in 2007. The National Water Resources Study (GOM 2000) predicted the Langat Basin would require an increase of 20 % in water demand by 2012 against a present supply of 1.0 Mm^3/day. Ngah

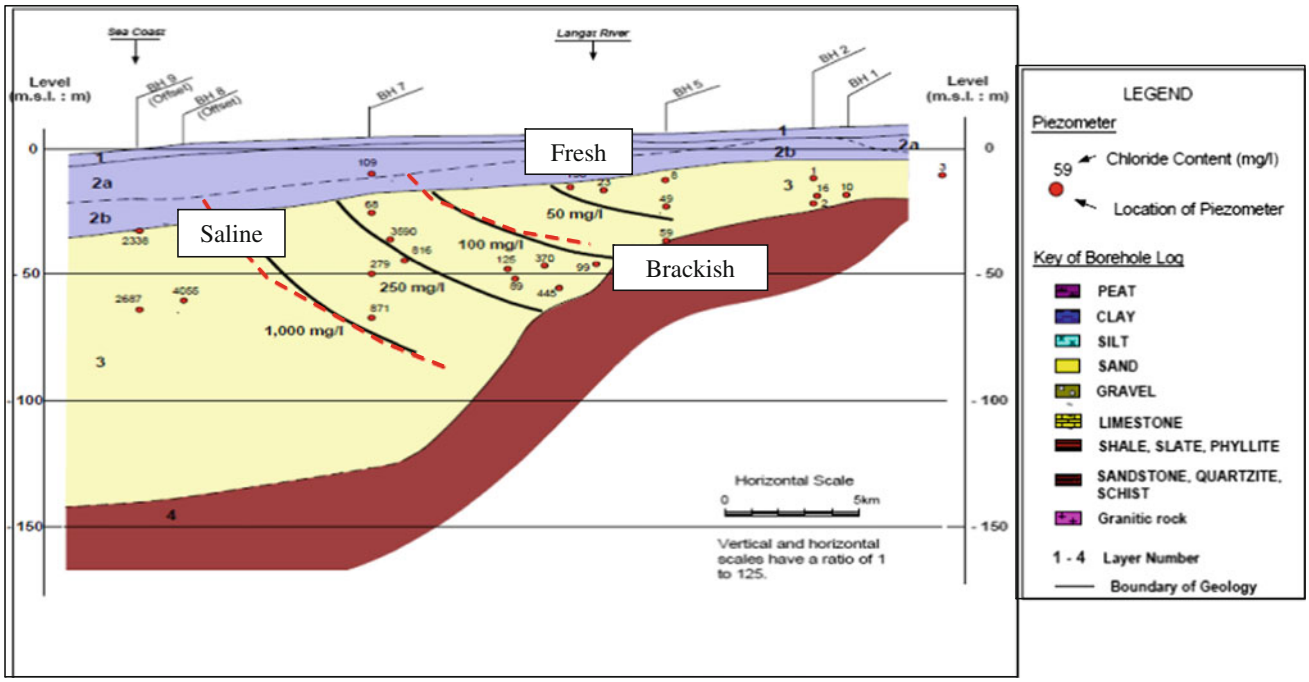

Fig. 4 Chloride distribution within the aquifer. Note the inclined saline–freshwater interfaces

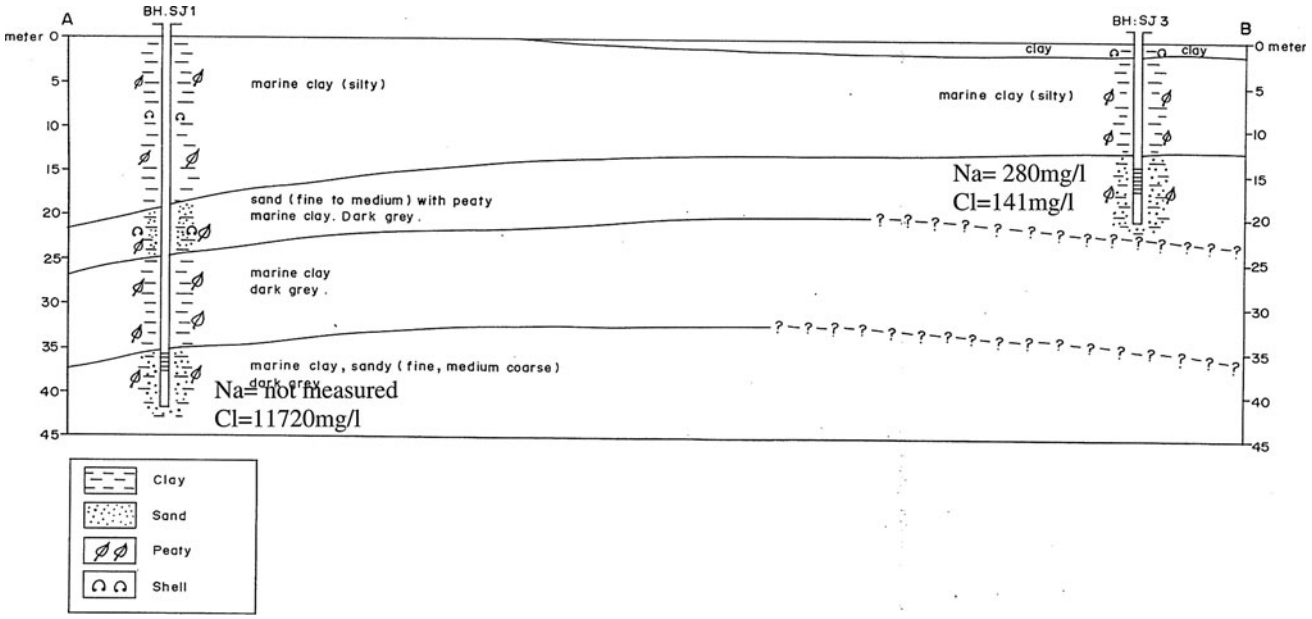

Fig. 5 Geochemistry data distribution in subsurface profile *A–B* of the semi-confined aquifer in Sg. Judah Village (after Ngah 1988)

(1988) in his study of the island's hydrogeology concluded that groundwater in the shallow semi-confined aquifers was enough for the need of the aborigine villages of Sg. Judah and Sg. Rambai (Figs. 1, 2). Exploration works carried out by some government agencies show that the island's deep aquifer has groundwater mixed with freshwater and saline–brackish water (Abdul Hamid 2003; Ismail 2008).

Materials and methods

Eight monitoring wells (Fig. 2) were installed in the unconfined aquifer: four (MW6, MW11, MW12, MW13) in the northwest in the mangrove preserved area, and four (MW5, MW7, MW10, and MW14) in the southeast in the heavily eroded area without mangrove. Additionally six

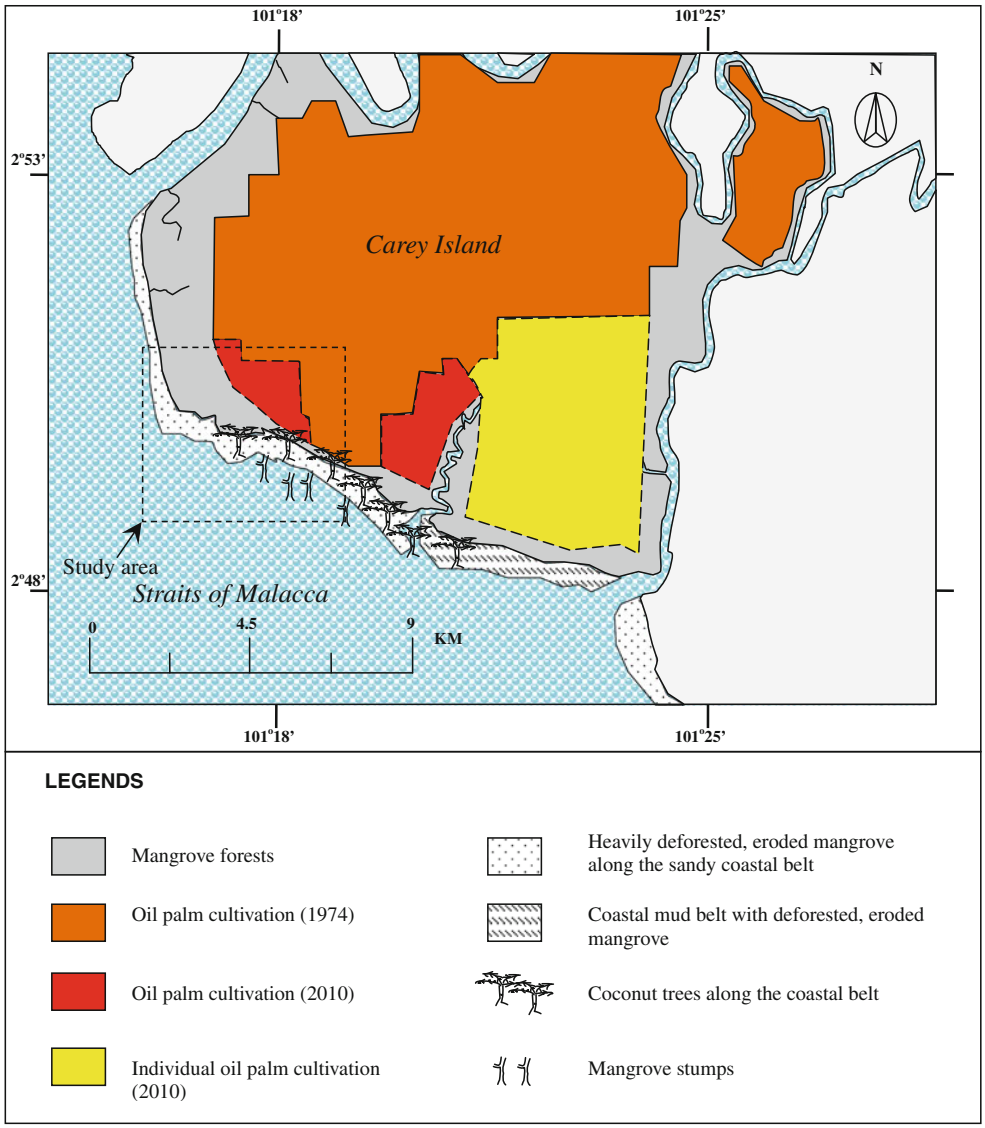

Fig. 6 Carey Island's land use as of 1974 and modern day; note vast oil palm cultivation (OPC) especially in the south and heavily deforested, eroded mangrove in the seawater-exposed coastal belt

other wells (MW1, MW2, MW3, MW4, MW8, and MW9) were installed in the semi-confined aquifer in the southwest of the semi-confined aquifer. The wells reached various depths (40, 50, and 80 m), respectively, with open screens installed in the 34–36, 47–49, and 67–69 m depths for groundwater quality sampling. Soil samples collected from the each of the well boreholes by rotary-washing were visually examined and laboratory analysed. Soil classification followed the BS 1377 (1990): fine sand (0.063–0.1 mm); medium sand (0.1–0.4 mm); and coarse sand (1–2 mm). Tests on the soil physical properties included particle-size distribution, Atterberg limit, moisture content, specific gravity, and linear shrinkage.

Earth resistivity and geo-chemical survey

Earth resistivity (ER) was measured following the traverse set up (Fig. 2) using a resistivity meter (ABEM Terrameter SAS4000 with electrode selector ES10-64). Spread in two phases, the first phase data were collected in August 2009, November 2009, and February 2010, and the second phase data in December 2010. The former data were used to establish a TDS–ER relationship in the vertical profile of the study area; whereas the latter data were used to map out the subsurface resistivity in the horizontal profile.

Groundwater monitoring was done once or twice a week, starting August 2009 until March 2011. Groundwater

samples were collected from the monitoring wells using a bailer. Four groundwater quality parameters (conductivity, salinity, TDS, and temperature) were measured using a water quality checker (YSI EC300) immediately after sampling. The equipment pre-calibrated against a standard potassium chloride solution (conductivity 1.411 mS/cm) in accordance with the APHA (2005) procedures.

In the first phase, nine resistivity lines L18–L18′, L19–L19′, L17–L17′, L5–L5′, L4–L4′, L20–L20′, L3–L3′, L2–L2′, and L12–L12′ were set up, each crossing, respectively, MW3, MW4, MW5, MW6, MW7, MW8, MW10, MW11, and MW12. No resistivity lines were set up crossing other wells (MW1, MW2, MW9, MW13 and MW14). In the second phase, a number of 17 resistivity lines, L1–L17, were set up, and the lines crossing the wells were as indicated above for the first phase and those not crossing other wells are as shown in Fig. 2.

All the 17 resistivity lines were each laid into the ground surface almost perpendicular to the shoreline (Fig. 2): 14 lines in the N–S direction, and 3 in the W–E direction of the study area. Each resistivity line (cable) was 400-m long, divided into four sections each 100-m long (designated as 1st, 2nd, 3rd, and 4th cables). Using an initial electrode spacing of 5-m intervals (for the middle 2nd and 3rd cables) and 10-m intervals (for the end 1st and 4th cables), ten electrodes were pegged each on the end 1st and 4th cables, and 20 electrodes each on the middle 2nd and 3rd cables, making a total of 61 electrodes for each 400 m survey cable. The spacing flexibility afforded by the Wenner array could thus propagate increasingly denser resistivity in the vertical resistivity image profile near the subsurface (Hamzah et al. 2006).

In the analysis, the measured resistivity data, which were merely apparent, were subjected to inversion that resulted in a model of subsurface resistivity which approximated the true subsurface resistivity distribution as described by Loke (2010a). The inversion was made possible using software RES2DINV as previously described by (Dahlin and Loke (1998) and Loke et al. (2003).

In using the inversion technique, each entire profile block was divided into a number of rectangular model cells based on the spread of the measured data (Loke and Barker 1996). The data inversion was executed using the smoothness-constrained least square method (deGroot-Hedlin and Constable 1990; Sasaki 1992) where the block's resistivity values (model parameters) were adjusted iteratively to obtain a true distribution of resistivity (model response). The model parameters and response were linked via a finite-difference method as described by Dey and Morrison (1979). Thus the differences between the calculated and measured data in an initial model were minimised using the root-mean-squared (RMS) method, and the iteration was continued to an RMS error limit of <5 % (Awni 2006), which was considered acceptable. However, the model with the lowest RMS error is not always the most appropriate as it can induce unrealistic variations in the resistivity model (Loke 2010b). In the study connection, the study area's topography was assumed flat (based on evidently small topographical variations <1.0 m as shown in Fig. 7), which affected the resistivity model insignificantly, thus warranting the use of the finite-difference method. The flat topography assumption therefore did not jeopardise the integrity of the results of the actual resistivity image.

Results and discussion

Two types of aquifers have been previously identified (Mohamad Faizal et al. 2011): an unconfined aquifer (in the present study area), 10–60 m thick, about 1.5 km into the sea, following analyses of MW5, MW7, MW10 (southeast) and MW6, MW11, MW12, MW13, and MW14 (northwest); and a semi-confined aquifer (outside of the present study area but further away into the sea), following analyses for MW2, MW3, MW4, MW8, and MW9 (Fig. 7). Mohamad Faizal et al. (2011) found freshwater in the unconfined aquifer to a maximum depth of 30 m with TDS < 1,000 mg/L.

The semi-confined aquifer exhibited fine-to-medium light-grey sand with coarse sand and gravel, impermeable materials (silt/clay), and shell fragments. The shells, found in MW5 and MW12, provided confirmatory evidence of the origin of the alluvial deposits from the marine environment (Gula Formation) (Fig. 7). The aquifer has an upper and a lower layer: the upper (20–30 m thick) is semi-impermeable in the 27–32 m zone with light clay, marine and silt clay; and the lower has fine-to-coarse light-grey sand and gravel. Additional analyses of MW1 and MW2 indicate that the upper layer had a maximum depth of 60–66 m, overlying a thin semi impermeable layer (3–5 m thick) in the lower layer (Fig. 7) whose thickness was not determined because of limitation in the borehole depth. Ngah (1988) also found in the semi-confined aquifer the presence of localised freshwater in shallow wells (<15 m deep) with chloride concentration <250 mg/L and brackish–saline water in depth shallower than 15 m. In Fig. 2 is shown the interface separating the upper unconfined aquifer from the upper semi-confined aquifer.

Groundwater tables and TDS monitoring

In Figs. 8 and 9 are shown the results of groundwater monitoring in the unconfined aquifer. The groundwater levels increased in the wet season but decreased in the dry season, indicating the unconfined layer responded more quickly to the local seasonal conditions than to the Langat

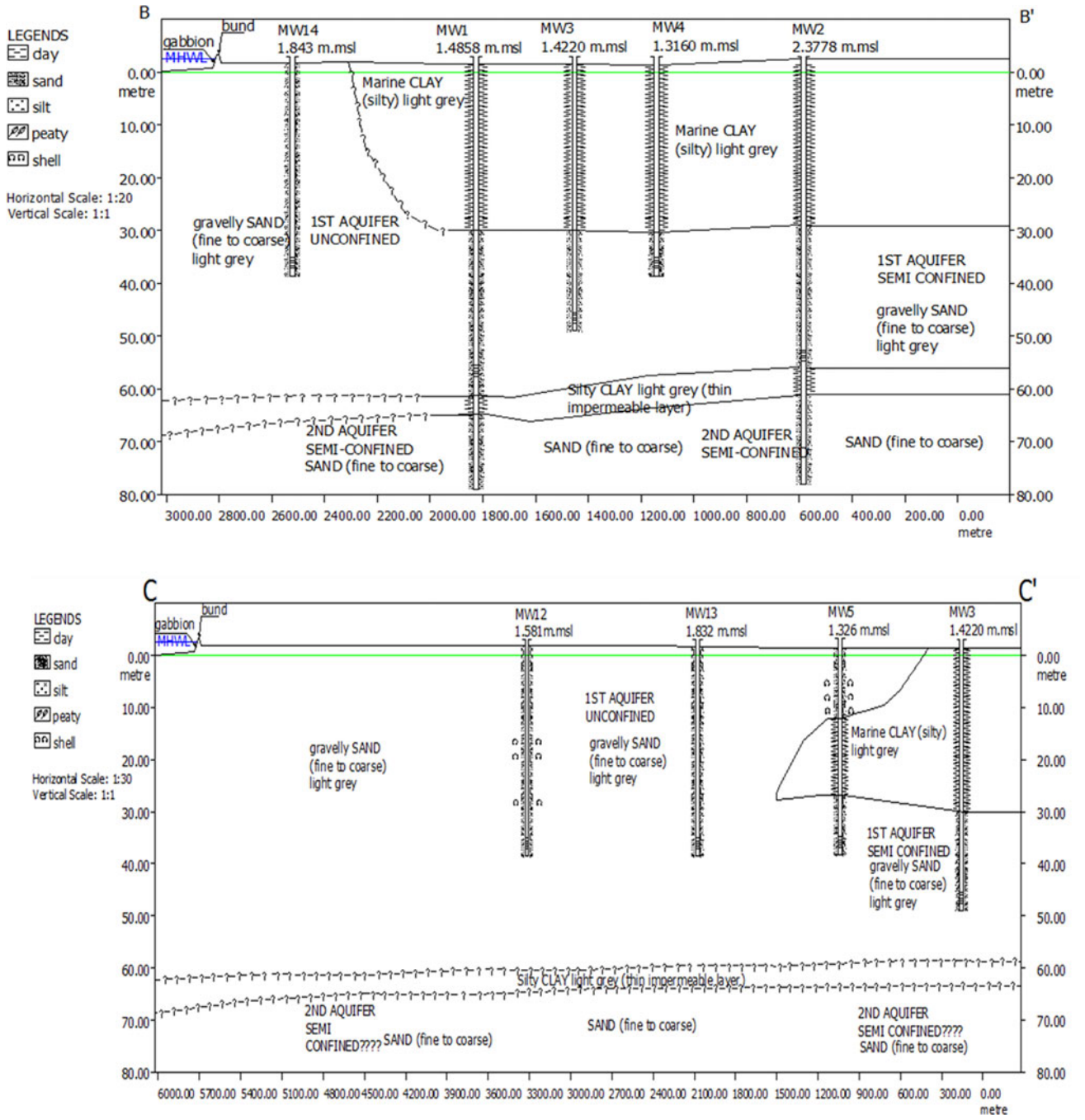

Fig. 7 Subsurface profiles, cross-sections *B*–*B*′ and *C*–*C*′, showing, respectively, the unconfined and confined aquifers. Note the shell fragments found in MW12 and MW5 (cross-section *C*–*C*′) confirm the quaternary alluvium deposits (Gula Formation) originated from the marine environment

Basin seasonal conditions as previously indicated by JICA and DMGM (2002). Another indication is that groundwater recharge relied more on local precipitation than on base flow from the mainland.

Contrasting TDS results were observed in the two sites during periods of low groundwater tables: In the southeast site, TDS levels exceeded 20,000 versus 10,000 mg/L in the northwest site. The northwest groundwater tables were about four times (0.6–0.8 m msl) as large as southeast (0.15–0.2 m msl) during both the wet and dry seasons. These observations were caused by the groundwater density, rather than elevation and pressure difference of the two sites. Also observed was seawater intrusion dominancy in the southeast, which was due to mangrove deforestation. The TDS results were spatially limited and thus might not truly represent the extent of seawater intrusion occurring in

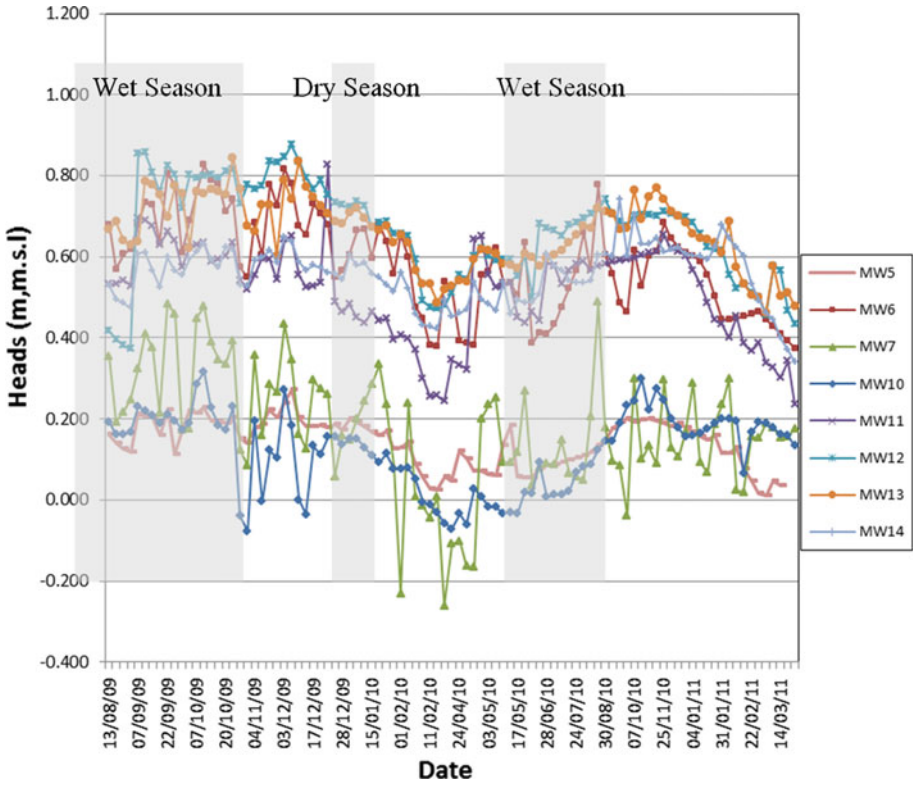

Fig. 8 High groundwater tables observed in MW12 (also in MW13, MW6, MW14, MW11, MW5, MW7, and MW10)

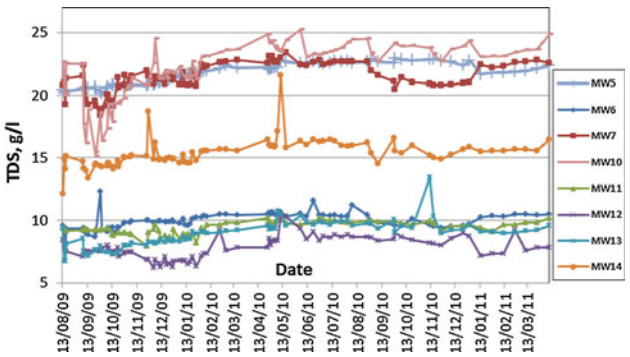

Fig. 9 Higher TDS values contradicting high groundwater tables in the monitoring wells (Fig. 8)

the study area. Thus to overcome this shortcoming, a resistivity contour mapping technique was attempted.

Correlation between water types and earth resistivity

The results of resistivity image showed low resistivity (<3 Ω m) in over 80 % of the image obtained (Fig. 10). Resistivity profile L5–L5′, however, showed higher resistivity (1.0–24.0 Ω m). Higher resistivity ranges have been reported for island coastal areas in other studies; for example, 0–1,000 Ω m (Wilson et al. 2006) and 0–2,500 Ω m (Pujari and Soni 2008). Wilson et al. (2006) in their study on marine sand derived a formation factor from consideration of measured pore-fluid resistivity and estimated bulk resistivity, which could be used as first approximation of pore-fluid resistivity (hence determination of water types) in future resistivity surveys. Pujari and Soni (2008) found a narrow resistivity band existed in an Indian coastal limestone area with resistivity from nearly 0–3.0 Ω m, which was interpreted to represent seawater. In the local (Malaysia) studies, Nawawi et al. (2001) interpreted resistivity of <5 Ω m to represent saline water in the western coast of Peninsular Malaysia; while Surip (1994) suggested resistivity <2 Ω m to represent alluvial salinity in the eastern coast.

Various underlying assumptions were used in the present study. Very low resistivity (from nearly zero to 3.0 Ω m) was taken to represent saline water and higher resistivity (3.0–24.0 Ω m) represented a mixture of freshwater and seawater. Since the Island's alluvial Quaternary is comprised of homogenous water-bearing sand and some gravel (due to large volumes of pore fluids), large volumes of groundwater could presumably flow through the fluid pores, thus causing resistivity to be affected more by the pore fluids rather than by the mineral soil composition, which in turn might allow the resistivity image of water types to be more apparent. The procedures for obtaining the water types from resistivity survey are available (Cartwright and McComas 1968; Ebraheem et al. 1990; Sherif et al. 2006; Mohamad Faizal et al. 2011; Ebraheem et al. 2012). In this study groundwater specific conductance was assumed as the reciprocal of water resistivity $\rho_w = 1/\sigma_w$ while soil conductance as the inverse of earth resistivity $\sigma_s = 1/\rho_e$.

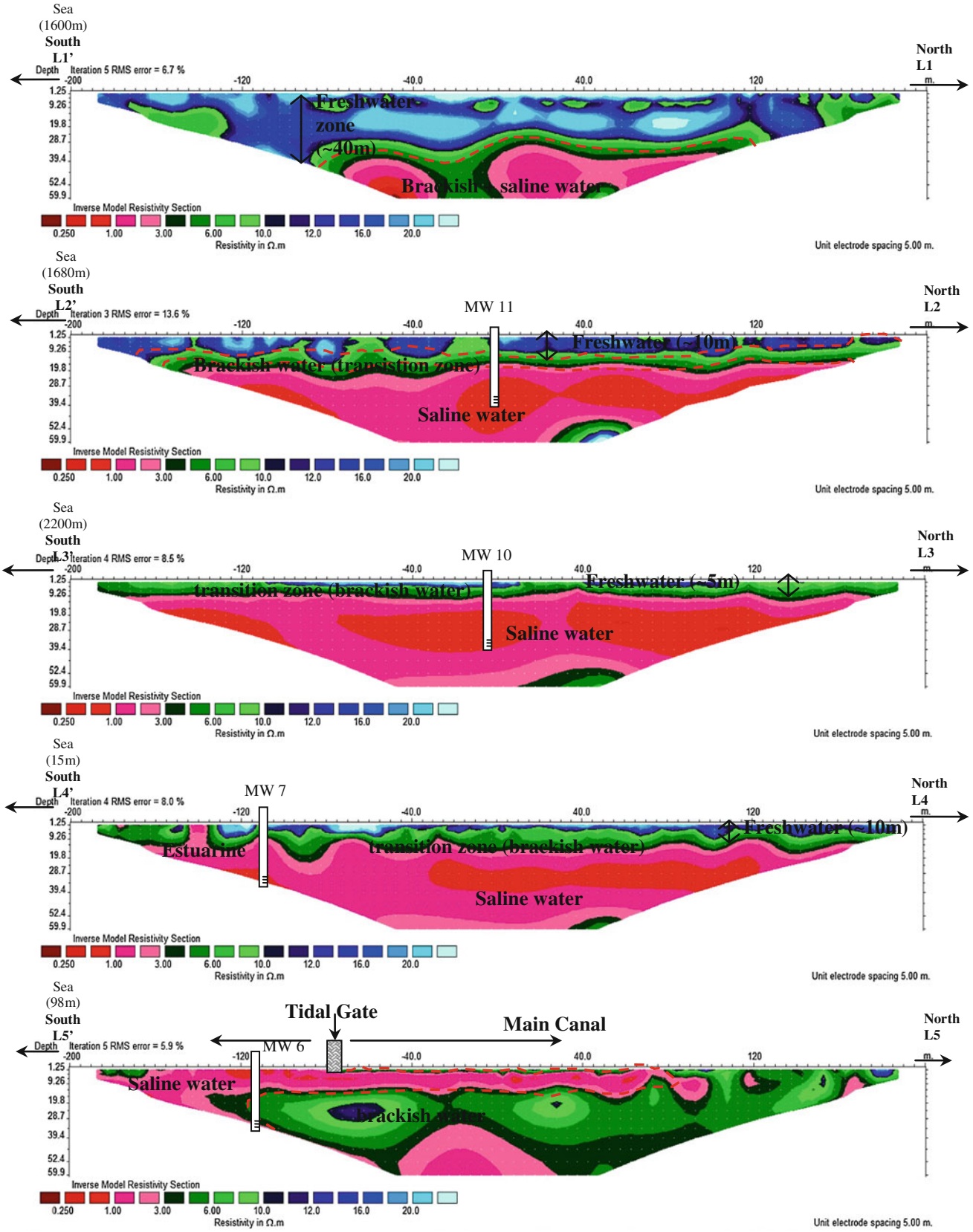

Fig. 10 True inverted resistivity profiles for L1–L1′, L2–L2′, L3–L3′, L4–L4′ and L5–L5′

Table 1 Measured groundwater conductivity, resistivity, and TDS and calculated soil conductivity and groundwater resistivity for determining the empirical relationships between earth resistivity and water resistivity and between TDS and earth resistivity

Well ID	Sampling Time (months)	Measured ground water table from ground surface (m)	Measured ground water table above msl (m)	Measured groundwater conductance (μS/cm)	Calculated soil conductance (μS/cm)	Calculated water resistivity (Ω m)	Measured resistivity (Ω m)	Measured TDS (mg/L)
MW3	Aug-09	0.942	0.480	35,240	9,083	0.2838	1.101	21,410
MW5	Aug-09	1.070	0.256	33,280	9,497	0.3005	1.053	20,330
MW6	Aug-09	0.944	0.530	14,870	3,211	0.6725	3.114	8,940
MW7	Aug-09	1.496	0.057	35,270	10,384	0.2835	0.963	21,190
MW8	Aug-09	0.999	0.492	23,010	5,173	0.4346	1.933	13,810
MW10	Aug-09	1.135	0.256	34,650	18,904	0.2886	0.529	21,060
MW11	Aug-09	1.150	0.712	27,250	8,197	0.3670	1.22	16,620
MW12	Aug-09	0.738	0.843	12,620	2,289	0.7924	4.368	7,660
MW3	Nov-09	0.964	0.458	34,420	11,099	0.2905	0.901	21,090
MW4	Nov-09	1.025	0.291	34,710	11,614	0.2881	0.861	21,420
MW6	Nov-09	0.770	0.704	15,790	3,212	0.6333	3.113	9,750
MW7	Nov-09	1.560	–0.007	34,720	9,785	0.2880	1.022	21,480
MW8	Nov-09	1.014	0.477	29,121	6,954	0.3434	1.438	18,050
MW10	Nov-09	1.160	0.231	33,930	13,850	0.2947	0.722	20,690
MW11	Nov-09	1.516	0.346	25,920	9,524	0.3858	1.05	16,120
MW3	Feb-10	1.117	0.305	36,890	11,905	0.2711	0.84	21,680
MW4	Feb-10	1.226	0.090	33,030	14,045	0.3028	0.712	19,430
MW5	Feb-10	1.277	0.049	37,990	13,908	0.2632	0.719	22,350
MW6	Feb-10	1.061	0.413	17,581	3,591	0.5688	2.785	10,340
MW7	Feb-10	1.490	0.063	38,640	24,450	0.2588	0.409	22,800
MW10	Feb-10	1.386	0.005	39,380	18,051	0.2539	0.554	23,250
MW11	Feb-10	1.183	0.679	35,842	16,694	0.2790	0.599	21,090
MW12	Feb-10	1.021	0.560	15,731	3,724	0.6357	2.685	9,220

Ebraheem et al. (1997, 2012) and Sherif et al. (2006) suggested that the geochemical and geophysical data might be correlated to obtain an empirical relationship if dissolved ions were found in the pore fluids rather than in the host soil, which was important for controlling the electricity-transmitting ability of groundwater according to Sherif et al. (2006). In this study, an empirical relationship between TDS and earth resistivity has been obtained (see Eq. 1), by which three TDS-based water types could be identified following classification by Fetter (2002): saline water (TDS > 10,000 mg/L), brackish water (1,000 < TDS < 10,000 mg/L), and freshwater (TDS < 1,000 mg/L).

Topographically, the study area was assumed flat, by which all measurements of the groundwater table levels were referred from the ground surface. High groundwater tables (0.461–1.560 m msl) were observed (Table 1). The inversion resistivity model (Fig. 10) used the Wenner array configuration, by which the smallest electrode spacing selected was found to be 5 m, which resulted in the resistivity image to start at the 2.50 m depth; this means the resistivity profile below the 2.5-m depth was taken as fully saturated with groundwater. Apart from the wells installed in the unconfined aquifer (study area) for correlation evaluation, MW3 and MW4 were also investigated for the same purpose, although located in the semi-confined aquifer [having water-saturated sandy soil properties similar to the unconfined aquifer in the same geological (Gula) formation]. These wells, MW3 and MW4, had screens installed at the 46–48 and 34–36 m depths, respectively, in the sand layer of the upper aquifer. The data measured and calculated for these wells are shown in Table 1.

Statistical analyses of the measured groundwater conductivity, resistivity, and TDS plus calculated soil conductivity and groundwater resistivity indicate the skewness and kurtosis for each data set were both within −1 to +1. Also a linear relationship was obtained as indicated by the Pearson correlation coefficient (r) between −0.9 and +0.9. The result indicates the data tested could be linearly related.

Graphical plots of water resistivity versus earth resistivity (Fig. 11) indicated the best-fit straight line could be described by the following relationship ($r^2 = 0.9593$):

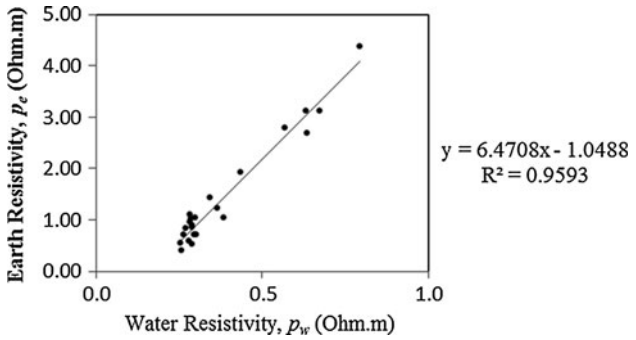

Fig. 11 Earth resistivity versus water resistivity

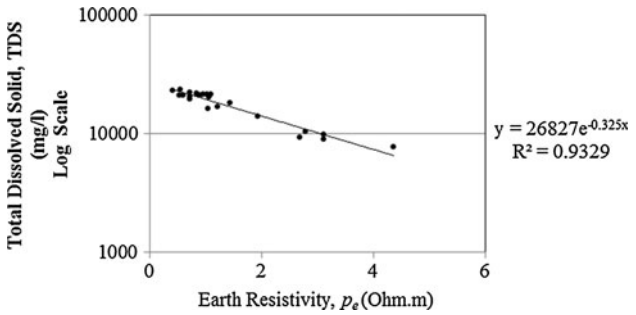

Fig. 12 Plot of TDS versus earth resistivity

$$\rho_e = 6.4708\rho_w - 1.0488 \quad (1)$$

where ρ_e is the earth resistivity (Ω m), and ρ_w is the water resistivity (Ω m).

The above analyses reveal that earth resistivity of the Quaternary alluvium aquifer and that of the saturated groundwater could affect salinity, thus reaffirming the basis for applying the geoelectrical–geochemical method in the study of seawater intrusion in the Island.

TDS and earth resistivity were also plotted (Fig. 12), giving the best-fit regression line of the following empirical relationship:

$$\log \text{TDS} = -0.1411\rho_e + 4.4286. \quad (2)$$

Using the TDS levels in the Fetter (2002) classification described above, the relationship as presented by Eq. 2 can be used to predict the resistivity values. Generally, such a relationship depends on sediment type and pore-water conductivity. Archie (1942) showed that using these considerations, the electrical conductivities of water (σ_w) and of linear formation (σ_f) might be related as described by Eq. 3:

$$\sigma_w = F\sigma_f. \quad (3)$$

Note F, the proportionality constant (or formation factor), relates to the sediment porosity. Equation 3 is valid for sediments whose matrix resistivity is high and the main conductor of electricity is pore-water. Poulsen et al. (2010) suggested that clay—if present in significant amount in the soil sediments—could be a significant conductor. Consequently, formation resistivity could become a non-linear function of pore-water conductivity, especially in the presence of freshwater with conductivity <0.5 S/m.

Equation 2 was used for the unconfined aquifer system containing granular material saturated with water. For MW3 and MW4, the sub-surface profile showed a marine clay layer to a depth of 30 m. Note that Eq. 2 is only applicable for depths between 30 and 64 m in the sandy soil of the Gula Formation.

Resistivity images (inverted 2D)

In Fig. 10 are shown the results of resistivity profiles for the five traverse lines using the inversion model (RES2DINV) software. Note that all profiles started at the 2.5-m depth measured from the ground surface. The results of groundwater table monitoring are shown in Table 1. The resistivity profiles selected in the five different locations, outlined below, are so selected as to represent variations in the two distinctively different land cover settings overlying the unconfined aquifer.

(a) Profile L1–L1′ is located in the mid-aquifer with mangrove cover in the west and south.
(b) Profile L2–L2′ is located in the west of the aquifer with mangrove cover.
(c) Profile L3–L3′ is in the middle east of the aquifer with open mangrove area in the east and south.
(d) Profile L4–L4′ is located close to heavily eroded coastal belt in the south.
(e) Profile L5–L5′ is located close to the estuary where the agriculture hydraulic structures (tidal gate, bund, and main canal) are found.

Three colour codes (blue, green, and red) are used to denote the different water types (respectively freshwater, brackish water, and saline water) as apparent in the resistivity image. Inserting the measured TDS values in Eq. 2, the resistivity values were predicted, from which the water types were determined according to the set colour coding with the designated range of resistivity values. The results obtained are as follows: fresh water ($\rho_e > 10.0\,\Omega$ m); brackish water ($3.0 < \rho_e < 10.0\ \Omega$ m), and saline water ($\rho_e < 3.0\ \Omega$ m).

Resistivity profile L1–L1′

This profile (Fig. 10) is, respectively, 1.6 and 2.5 km from the south and west of the study area. Freshwater thickness (blue coded) varied in depth from 28 m (minimum) to 40 m (maximum) with the overall resistivity within the freshwater lens ranging from 10 to 55 Ω m. Below the

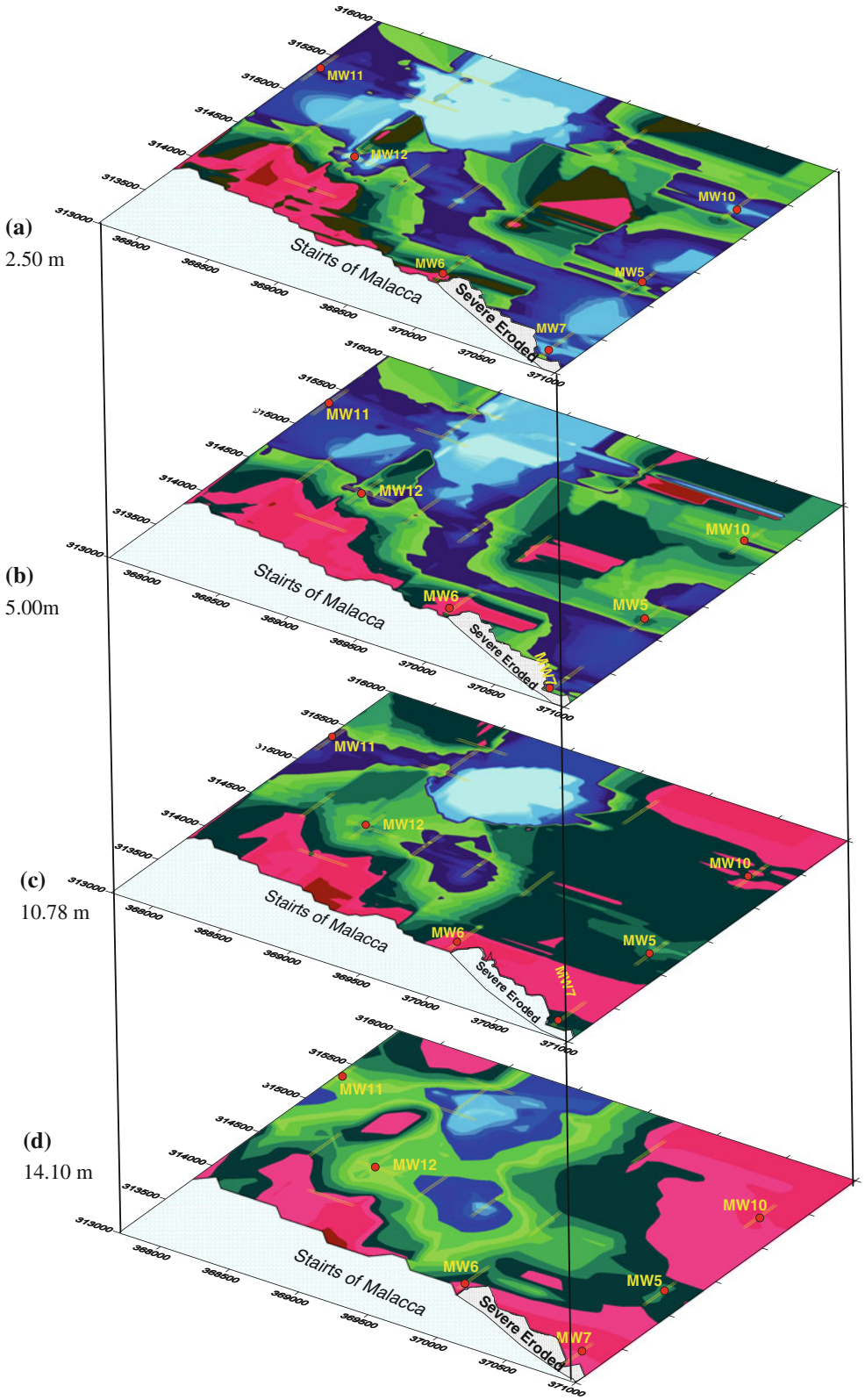

Fig. 13 Horizontal profiles of true (inverted 3D) resistivity distribution

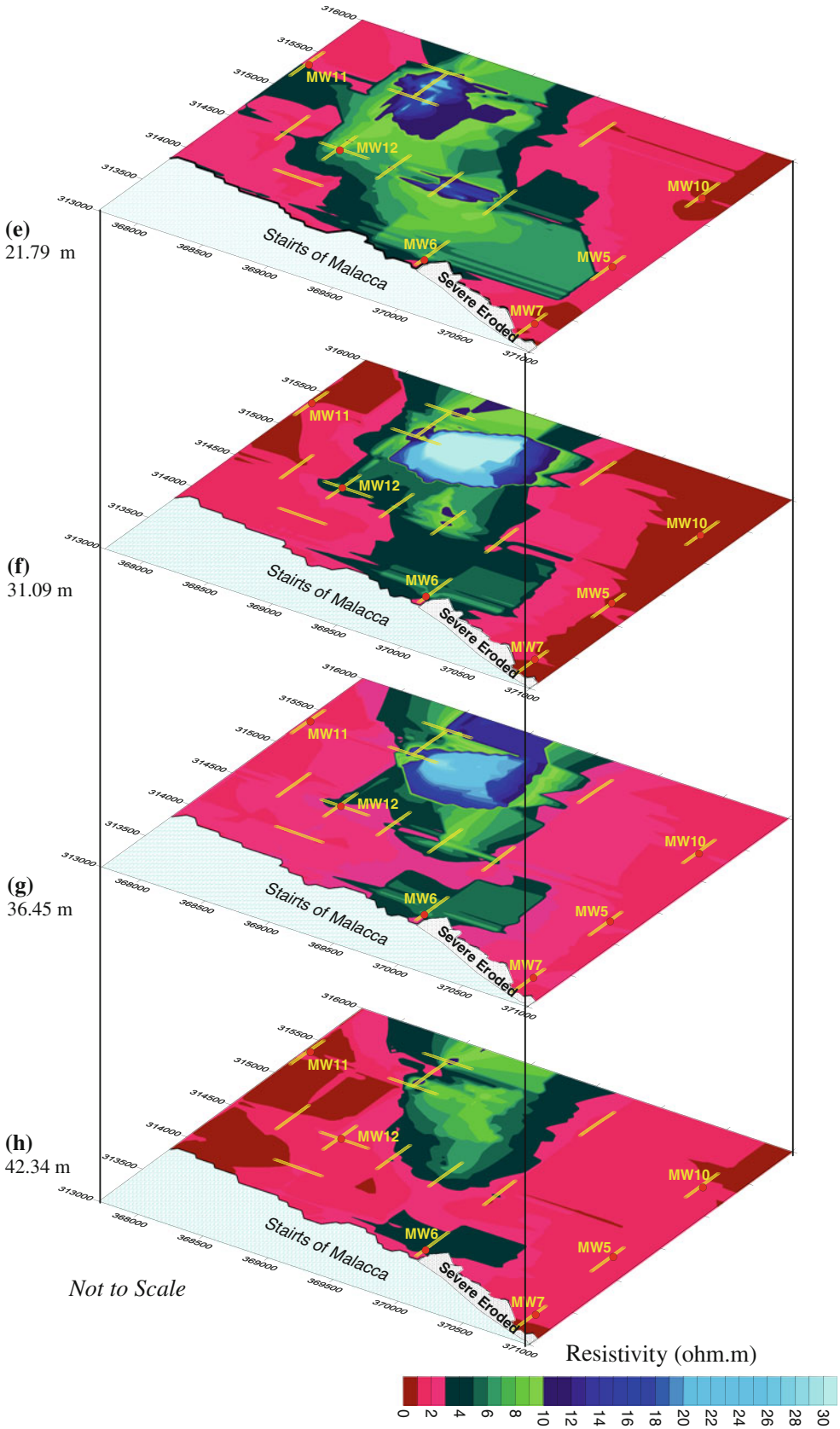

Fig. 13 continued

Table 2 Summary of water types and area coverage/dominancy

Vertical depth of water zone (m)	Horizontal area coverage (km^2) of water types		Freshwater area dominancy	Remarks
	Freshwater, >10 Ω m Blue	Brackish–saline water, ~0–10 Ω m Green–Red		
2.5	3.50	6.89	West to East	Brackish–saline water caused by seepage from main canal and agriculture drainage (Fig. 13a)
5.0	3.25	7.13	West and Middle	Brackish–saline water caused by seepage from main canal and agriculture drainage (Fig. 13b)
10.78	1.00	9.38	Middle	Brackish–saline water caused by seawater intrusion mostly from severely eroded area (east) (Fig. 13c)
14.10	0.75	9.63	Middle	Brackish–saline water caused by seawater intrusion mostly from severely eroded area (east) (Fig. 13d)
21.79	0.40	9.78	Middle	Brackish–saline water caused by seawater intrusion (Fig. 13e)
31.09	0.38	10.00	Middle	Brackish–saline water caused by seawater intrusion (Fig. 13f)
36.45	0.35	10.03	Middle	Brackish–saline water caused by seawater intrusion (Fig. 13g)
42.34	–	10.38	–	Brackish–saline water caused by seawater intrusion (Fig. 13h)

freshwater was found brackish water (green coded) overlying saline water (red coded) separated by an undulating saline–brackish water interface.

Resistivity profile L2–L2′

This profile (Fig. 10) crossed MW11 at mid-survey line, traversing from the mangrove into the oil palm cultivation area (Fig. 2). Freshwater lenses were scattered about throughout the cross-section in approximately 10 m thickness with resistivity between 10.0 and 24 Ω m. Saline water (red coded) was dominantly found in the 19-m depth (with resistivity below 3 Ω m) overlain by brackish water (green coded). These water types exhibited almost horizontal interfaces between each other.

Resistivity profile L3–L3′

This profile (Fig. 10) crossed over MW10 in the mid-profile (Fig. 2). The nearest coastal area to the study area was about 2.2 km away in the south beneath the open mangrove with severely eroded land cover. Brackish water (green) was thin, overlying the saline water (red coded) which was predominantly found with low resistivity (below 3 Ω m) below the 10-m depth. The freshwater lens appeared only 5 m thick.

Resistivity profile L4–L4′

This profile (Fig. 10) located 15 m away from the coast crossed over MW7 (Fig. 2). In the distance about 3.2 km landward was found coastal mangrove, heavily deforested and eroded. Freshwater was <10 m thick with resistivity exceeding 10.0 Ω m. The saline water was, however, more prominent in the subsurface with low resistivity (<3 Ω m).

Resistivity profile L5–L5′

This profile (Fig. 10), about 98 m away from the coast, crossed over MW6 (Fig. 2). Close to it were found some of the estuarine hydraulic structures such as open canals and tidal gates. In the shallow subsurface was saline water 2.5–10 m deep with resistivity between 0.5 and 3 Ω m. Brackish water was predominant below the saline water in the 400-m distance of the traverse line with resistivity between 3 and 10 Ω m. This explains why the freshwater was saline in the estuarine canals.

In relative profile comparison, it is noted that all profiles had freshwater in varying thickness except L5–L5′. Profiles L2–L2′; L3–L3′; and L4–L4′ appeared to have thinner freshwater compared with L1–L1′. Both L3–L3′ and L4–L4′, it is noted, were located in the eroded side (west) of the study area. Profile L1–L1′ has practical implication in that freshwater production wells could be constructed in the vicinity of the traverse line at depths exceeding 20 m as compared with the shallower wells for all other profiles.

Resistivity image (inverted 3D)

Resistivity distribution was spatially analysed by interpolation using the Kriging technique available in Surfer 8. The true (inverted 2D) vertical profiles (Fig. 10) were converted into true (inverted 3D) horizontal profiles, shown in Fig. 13 for selected depths. Although the 3D images have apparently limited resolution due the limited number of profiles examined in comparison with the survey area

(30 km^2), the method has produced sufficiently better resistivity distribution of the different water types.

The results of the water types (3D) are summarised in Table 2 with reference to water depths. The colour codes used are blue for freshwater (>10 Ω m), green for brackish water (3–10 Ω m), and red for saline water (<3 Ω m). The following discussion is only confined for demonstrative purpose for the 2.5–5.0 m depth (Fig. 13a, b) of the unconfined aquifer. In this water zone freshwater (horizontal) coverage is about 3.0 km^2, half of the coverage for brackish–saline water (about 7.0 km^2). The dominancy of water brackishness/salinity was due to seepage from the irrigation canals [profile L6–L6′ (near MW6), profile L7–L7′ and profile L8–L8′ shown in Fig. 6]. The freshwater contamination in the shallow aquifer was believed to be caused by seawater infiltrating from the irrigation canals. In the same depths (2.5–5.0 m) the saline water occurred mostly in the southwest (in the reserved mangrove) due to tide moving from the mangrove to the bunds separating it from the oil palm cultivation. In the past the bunds in the mangrove have been frequently damaged, causing the saline water to overflow into the oil palm plantation, thus contributing to the groundwater salinity in the southwest area. An important finding in the study is the indication of freshwater availability in the mid-study area as deep as 30 m into the aquifer beneath the mangrove (Fig. 13). For depths exceeding 10 m the saline water occurrence was mainly due to seawater intrusion (Table 2).

Conclusion

Land transformation from severe mangrove deforestation in the southeast of the study area close to the resistivity profile L16–L16′ crossing MW7 has resulted in major coastal erosion in the study area, reducing topography down to the original coastal surface level, as well as shifting seawater intrusion farther into the land mass compared with the time when mangrove was still intact. The geo-electric and geo-chemistry integrated method has been demonstrated as an effective tool in defining the freshwater lens morphology affected by seawater intrusion and agriculture irrigation saline water. The freshwater potential zone was 30 m below the ground surface in the unconfined aquifer under close proximity of the preserved mangrove forest, which was fourfold thicker than beneath the severely eroded mangrove barren coastal belt. The seawater intrusion exhibited more severe effect in the 10 m depth of the unconfined aquifer on the eastern side facing the heavily eroded area as compared with the western side in the same depth (Fig. 13c). For depths exceeding 42 m, the brackish–saline water was found dominant in the entire unconfined aquifer (Fig. 13h). The agriculture saline water has affected the freshwater at the 5-m depth close to the irrigation canals located parallel to the resistivity profiles L13–L13′, L14–L14′, and L15–L15′ (Fig. 13a, b). These findings provide useful information for future groundwater supply planning in the study area subject to limited groundwater recharge that is dependent only upon local precipitation.

Acknowledgments The project has been made possible by a research grant provided by Institute of Ocean and Earth Science (IOES) University Malaya, Kuala Lumpur, Malaysia.

References

Abdul Nassir SS, Loke MH, Lee CY, Nawawi MNM (2000) Salt-water intrusion mapping by geoelectrical imaging surveys. Geophys Prospect 48(4):647–661. doi:10.1046/j.1365-2478.2000.00209.x. http://web.ebscohost.com/ehost/pdf?vid=3&hid=113&sid=f505c08d-d330-4dc5-99bo-df1909144ee2%40sessionmgr109. Accessed 4 Jan 2009

Adepelumi A, Ako BD, Ajayi TR, Afolabi O, Omotoso EJ (2009) Delineation of saltwater intrusion into the freshwater aquifer of Lekki Peninsula, Lagos, Nigeria. Environ Geol 56(5):927–933. doi:10.1007/s00254-008-1194-3. http://www.spingerlink.com/content/ekj1477561052r10/fulltext.pdf. Accessed 8 Jan 2009

Affandi NAM, Kamali B, Rozainah MZ, Mohd Tamin N, Hashim R (2010) Early growth and survival of *Avicennia alba* seedlings under excessive sedimentation. Sci Res Essays 5(18): 2801–2805. ISSN: 1992-2248 http://www.academicjournals.org/SRE. Accessed 2 Apr 2011

APHA (2005) Standard methods for the examination of water and wastewater (21st edn). American Public Health Association, Washington, DC. ISBN: 0-87553-047-8

Archie GE (1942) The electrical resistivity log as an aid in determining some reservoir characteristics. Trans AIME Eng 146:54–61. http://www.pe.tamu.edu/blasingame/data/z_zCourse_Archive/P663_03C/P663_03C_TAB_Ref_FormEval/SPE_Trans_1942_Archie_Reservoir_Char_from_Resistivity_Logs.pdf. Accessed 4 Jan 2011

Awni TB (2006) Use of electrical resistivity methods for detecting subsurface fresh and saline water and delineating their interfacial configuration: a case study of the eastern Dead Sea coastal aquifers, Jordan. Hydrogeol J 14:1277–1283. doi:10.1007/s10040-006-0034-3. http://www.spingerlink.com/content/956130034272326/fulltext.pdf. Accessed 28 Dec 2008

Baba MF (2003) Geology Quaternary at Teluk Datuk area, State of Selangor (Sheet 101). Geology Quaternary Report, Department of Mineral and Geoscience Malaysia, Ministry of Natural Resources and Environment Malaysia, pp 1–32

Baharuddin MFT, Hashim R, Taib S (2009) Electrical imaging resistivity study at the coastal area of Sungai Besar, Selangor, Malaysia. J Appl Sci 9(16):2897–2906. doi:10.3923/jas.2009.2897.2906, http://scialert.net/qredirect.php?doi=jas.2009.2897.2906&linkid=pdf. Accessed 27 Dec 2010

Benkabbour B, Toto EA, Fakir Y (2004) Using DC resistivity method to characterize the geometry and the salinity of the Plioquaternary consolidated coastal aquifer of the Mamora plain, Morocco. Environ Geol 45(4):518–526. doi:10.1007/s00254-003-0906-y. http://www.spingerlink.com/content/3ejfg3cn4t89r141/fulltext.pdf. Accessed 4 Jan 2009

British Standard (BS) 1377 (1990) Part 2: method of test for soils for civil engineering purposes. British Standard Institution, London, pp 1–68. ISBN: 0580178676

Cartwright K, McComas MR (1968) Geophysical surveys in the vicinity of sanitary landfills in northeastern Illinois. Ground Water 5:23–30. http://info.ngwa.org/GWOL/pdf/682578001.PDF. Accessed 27 Dec 2010

Dahlin T, Loke MH (1998) Resolution of 2D Wenner resistivity imaging as assessed by numerical modelling. Journal of Appl Geophys 38(4):237–249. pii:50926-9851(97)00030-X. http://www.sciencedirect.com/science?_ob=MImg&_imagekey=B6VFC-35x5299-8-1&-cdi=60078_user=15079. Accessed 8 Jan 2009

deGroot-Hedlin C, Constable S (1990) Occam's inversion to generate smooth, two-dimensional models from magnetotelluric data. Geophysics 55(12):1613–1624

Dey A, Morrison HF (1979) Resistivity modelling for arbitrarily shaped two-dimensional structures. Geophys Prospect 27(1):106–136. doi:10.1111/j.1365-2478.1979.tb00961.x. http://www3.interscience.wiley.com/user/ID=119598599&Act=21388code=4726&Page=/cgi-bin/fulltext/11. Accessed 8 Jan 2009

Di Sipio E, Galgaro A, Zuppi GM (2006) New geophysical knowledge of groundwater systems in Venice estuarine environment, Estuarine, Coastal and Shelf Science. 66:6–12. doi:10.1016/j.ecss.2005.07.015. http://www.sciencedirect.com/science?_ob=MImg&_imagekey=B6WDV-4H6PKWO-1-H&cdi=67768_user=15079. Accessed 6 Jan 2010

Ebraheem AM, Hamburger MW, Bayless ER, Krothe NC (1990) A study of acid mine drainage using earth resistivity measurements. Ground Water 28(3):361–368. http://info.ngwa.org/GWOL/pdf/901550570.PDF. Accessed 6 Jan 2010

Ebraheem AM, Senosy MM, Dahab KA (1997) Geoelectrical and hydrogeochemical studies for delineating groundwater contamination due to saltwater intrusion in the northern part of the Nile Delta, Egypt. Ground Water 35(2):216–222. http://info.ngwa.org/GWOL/pdf/971262673.PDF. Accessed 6 Jan 2010

Ebraheem AM, Sherif MM, Al Mulla MM, Akram SF, Shetty AV (2012) A geoelectrical and hydrogeological study for the assessment of groundwater resources in Wadi Al Bih, UAE. Environ Earth Sci. doi:10.1007/s12665-012-1527-0 (online first). http://www.springerlink.com/content/1308v2q248w76134/fulltext.pdf

Fetter CW (2002) Applied hydrogeology, 4th edn. Prentice Hall Inc., New Jersey, pp 1–598. ISBN: 0131226878

Golden Hope Plantation Berhad (2006) Carey Island; a golden heritage; reliving history, preserving legacy. Golden Hope Plantation Berhad, pp 1–16. ISBN: 967-969-547-6

Government of Malaysia (GOM) (2000) The National Water Resources Study 2000–2050, vol 1 (study undertaken by SMHB, Ranhill and Jurutera Perunding Zaaba), pp 1–78

Government of Malaysia (GOM) (2010) Tenth Malaysia Plan (2011–2015). The Economic Planning Unit (EPU) Prime Minister's Department Putrajaya 2010 Malaysia http://www.epu.gov.my/html/themes/epu/html/RMKE10/img/pdf/en/chapt4.pdf

Hamzah U, Yaacup R, Samsudin AR, Ayub MS (2006) Electrical imaging of the groundwater aquifer at Banting, Selangor, Malaysia. Environ Geol 49(8):1156–1162. doi:10.1007/s00254-005-0160-6. http://www.spingerlink.com/content/r8q5880065u3857/fulltext.pdf. Accessed 4 Jan 2009

IPCC (2007) Climate change 2007: impacts, adaptations, and vulnerability. Contribution of working group II to the fourth assessment report of the intergovernmental panel on climate change. Cambridge University Press, Cambridge. http://www.ipcc.ch/publications_and_data/publications_ipcc_fourth_assessment_report_wg2_report_impacts_adaptation_and_vulnerability.htm

Ismail R (2008) Construction and exploration of deep wells at Carey Island and Kg Kelanang, Kuala Langat District, Banting Selangor. National Groundwater Resources Study under Subproject groundwater resources for State of Selangor. Report done by KS Global Sdn Bhd with collaboration Multical Card (M) Sdn Bhd under instruction the Department of Mineral and Geoscience Selangor State, Malaysia

JICA and DMGM (2002) The study on the sustainable groundwater resources and environmental management for the Langat Basin in Malaysia. Japan International Cooperation Agency (JICA) and Mineral and Geoscience Department Malaysia (MDGM) report, vol 2, pp 1–240

Loke MH (2010a) Tutorial: 2-D and 3-D electrical imaging surveys, pp 1–145. (http://www.geoelectrical.com/downloads.php. Accessed 2 Apr 2011

Loke MH (2010b) RES2DINV ver. 3.59 for Windows XP/Vista/7 for rapid 2-D resistivity and IP inversion using the least squares method, pp 1–148. http://www.geoelectrical.com/downloads.php). Accessed 2 Apr 2011

Loke MH, Barker RD (1996) Rapid least squares inversion of apparent resistivity pseudosection using a quasi-Newton method. Geophys Prospect 44(3):131–152. GPPRAR44(1)1-178(1996). ISSN: 0016-8025

Loke MH, Acworth I, Dahlin T (2003) A comparison of smooth and blocky inversion methods 2-D electrical imaging surveys. Explor Geophys 34(3):182–187. http://www.geoelectrical.com/downloads.php. Accessed 2 Apr 2011

Maillet GM, Rizzo E, Revil A, Vella C (2005) High resolution electrical resistivity tomography (ERT) in a transition zone environment: application for detailed internal architecture and infilling processes study of a Rhone River paleo-channel. Mar Geophys Res 26:317–328. doi:10.1007/s11001-005-3726-5. http://www.spingerlink.com/content1y1x7m7247q5x40p6/fulltext.pdf. Accessed 6 Jan 2010

Mohamad Faizal TB, Samsudin T, Roslan H, Mohd Hazreek ZA, Mohd Fakhrurrazi I (2011) Time-lapse resistivity investigation of salinity changes at an ex-promontory land: a case study of Carey Island, Selangor, Malaysia. Environ Monit Assess J. doi:10.1007/s10661-010-1792-x. http://www.spingerlink.com/content/c672761301151461/fulltext.pdf. Accessed 8 Dec 2011

Nawawi MNM, Harith ZZT, Ayub MS, Ibrahim AN, Alphonse A (2001) Modeling of an undergroundwater aquifer using 2-D electrical imaging technique in Brooklands Plantation, Selangor, Malaysia. In: Proceedings of the second international symposium on geophysics, Egypt, pp 293–297

Ngah DS (1988) Groundwater investigation for determination of suitability using hand-pump at rural area of Kuala Langat District, Selangor Darul Ehsan, Report No. GPH1/1988. Department of Mineral and Geosciences Malaysia, Ministry of Natural Resources and Environment

Poulsen SE, Rasmussen KR, Christensen NB, Christensen S (2010) Evaluating the salinity distribution of a shallow coastal aquifer by vertical multielectrode profiling (Denmark). Hydrogeol J 18:161–171. doi:10.1007/s10040-009-0503-6. http://www.springerlink.com/content/h1362g6228613458/fulltext.pdf. Accessed 30 Oct 2010

Pujari PR, Soni AK (2008) Sea water intrusion studies near Kovaya limestone mine, Saurashtra coast, India. Environ Monit Assess 154(1–4):93–109. doi:10.1007/s10661-008-0380-9. http://www.spingerlink.com/content/5w365533728128x2/fulltext.pdf. Accessed 6 Jan 2010

Sasaki Y (1992) Resolution of resistivity tomography inferred from numerical simulation. Geophys Prospect 40:453–464

Sathish S, Elango L, Rajesh R, Sarma VS (2011) Assessment of seawater mixing in a coastal aquifer by high resolution electrical resistivity tomography. Int J Environ Sci Technol 8(3):483–492. ISSN: 1735-1472. http://www.ijest.org/jufile?c2hvd1BERj00OTc=&ob=21c1b0b6c9ad046f5fc53584f9143f30&fileName=full_text.pdf. Accessed 10 June 2011

Schneider JC, Kruse SE (2003) A comparison of controls on freshwater lens morphology of small carbonate and siliciclastic islands: examples from barrier islands in Florida, USA, J Hydrol

284:253–269. doi:10.1016/j.jhydrol.2003.08.002. http://www.sciencedirect.com/science?_ob=MImg&_imagekey=B6V6C-49V7C76-7-1H&_cdi=5811&_user=152948&_pii=S0022169403002944&_origin=search&_zone=rslt_list_item&_coverDate=12%2F22%2F2003&_sk=997159998&wchp=dGLbVtb-zSkzS&md5=eba19cc5ecdf99e2ba300d922e2d248e&ie=/sdarticle.pdf. Accessed 6 Jan 2011

Schneider JC, Kruse SE (2006) Assessing selected natural and anthropogenic impacts on freshwater lens morphology on small barrier Islands: Dog Island and St. George Island, Florida, USA. Hydrogeol J 14:131–145. doi:10.1007/s10040-005-0442-9. http://www.springerlink.com/content/v515467525r2n551/fulltext.pdf. Accessed 30 Oct 2010

Sherif M, El Mahmoudi A, Garamoon H, Kacimov A, Akram S, Ebraheem A, Shetty A (2006) Geoelectrical and hydrogeochemical studies for delineating seawater intrusion in the Outlet of Wadi Ham, UAE. Environ Geol 49(4):536–551. doi:10.1007/s00254-005-0081-4. http://www.spingerlink.com/content/7w07144t21663226/fulltext.pdf. Accessed 4 Jan 2009

Suntharalingam T, Teoh LH (1985) Quaternary geology of the coastal plains of Taiping. Quat Geol Rep. Geological Survey Malaysia. Ministry of Primary Industries Malaysia

Surip N (1994) Application of geophysical methods, hydrogeology and radioisotope for detecting saline groundwater aquifer at Kuala Rompin dan Marang of Eastern Peninsular Malaysia. MSc thesis, National University of Malaysia(unpublished)

Suratman S (2005) The study on sustainable groundwater resources and environmental management for the Langat basin in Malaysia. Groundwater intensive use, international association hydrogeologist (IAH) selected papers on hydrogeology, vol 7. Taylor and Francis Group, London, pp 341–350. ISBN: 041536442

Tahir H, Abdul Hamid I (2003) The study of groundwater resource at Teluk Gong, Pelabuhan Kelang, Selangor Darul Ehsan. Report No. JMG.SWP (HG) 03/2003. Department of Mineral and Geosciences Malaysia, Ministry of Natural Resources and Environment

Vaeret L, Kelbe B, Haldorsen S, Taylor RH (2009) A modelling study of the effects of land management and climatic variations on groundwater inflow to Lake St Lucia, South Africa. Hydrogeol J 17:1949–1967. doi:10.1007/s10040-009-0476-5. http://www.springerlink.com/content/k6n481h1p76x14p2/fulltext.pdf

Wilson SR, Ingham M, McConchie JA (2006) The applicability of earth resistivity methods for saline interface definition. J Hydrol 316:301–312. doi:10.1016lj.jhydrol.2005.05.004. http://www.sciencedirect.com/science?-ob=MImg&_imagekey=B6V6C-4GFCR6N-4-R&_cdi=5811&_user=15079. Accessed 6 Jan 2010